RSC Advances

PAPER

View Article Online
View Journal | View Issue

Cite this: *RSC Adv.*, 2020, **10**, 44892

Design, characterization and catalytic evaluation of halometallic ionic liquid incorporated Nd_2O_3 nanoparticles ([smim][$FeCl_4$]$^-$@Nd_2O_3) for the synthesis of *N*-aryl indeno pyrrole derivatives†

Mohd Umar Khan, Ryhan Abdullah Rather and Zeba N. Siddiqui *

Silica modified imidazolium [smim] based halometallic ionic liquids, [smim][MCl_4] (M = Fe, Cu and Zn), were synthesized for the evaluation of acidic and catalytic properties. Among these ILs, [smim][$FeCl_4$]$^-$ was used for the preparation of heterogeneous catalyst ([smim][$FeCl_4$]$^-$@Nd_2O_3) by simple immobilization of IL on Nd_2O_3 nanoparticles. The structure of [smim][$FeCl_4$]$^-$@Nd_2O_3 was established by various techniques including FTIR, Raman, UV-vis DRS, powder XRD, SEM/EDX, elemental mapping, TEM, TGA, EPR and XPS analyses. The stability of nano-catalyst, [smim][$FeCl_4$]$^-$@Nd_2O_3, was established with the help of zeta potential analysis which showed a value of −40.32 mV lying under the stability range. Potentiometric titration with *n*-butyl amine was used to evaluate the acidic properties of [smim][MCl_4] as well as [smim][$FeCl_4$]$^-$@Nd_2O_3. The catalytic potential of the material was probed through the one pot synthesis of *N*-aryl indeno pyrrole derivatives. The results showed excellent performance of the material by producing a high yield (98%) of indeno pyrrole derivatives. A recyclability experiment revealed that the catalyst was efficient in up to five cycles with insignificant loss in catalytic activity. The evaluation of green metrics indicated the sustainability of the present protocol in terms of high atom economy and low E-factor.

Received 16th October 2020
Accepted 3rd December 2020

DOI: 10.1039/d0ra08812a

rsc.li/rsc-advances

1. Introduction

Imidazolium ionic liquids (ILs) have emerged as outstanding ILs (functional material) due to the presence of a distinctive five membered imidazole ring. They offer several advantages such as better activity and reactivity than other ILs,[1] air and moisture stability *etc.*[2] Concerning the anionic part, ILs with chlorometallate anions are of great importance in Lewis acidic catalysis, ionothermal synthesis of semiconductors, gas storage systems and development of biomass processing.[3] In this regard, chloride salts of transition metals especially iron, cobalt, nickel, copper and zinc are widely used as a metal source in catalysis.[4–6] But, ILs in homogeneous catalysis suffer from demerits such as the use of large amounts of ILs as solvents or catalysts producing huge amounts of waste materials which are extremely difficult to dispose of and hence these processes cannot be considered as eco-friendly. Therefore, to evade the limitations of homogeneous catalysis using ILs and to introduce heterogeneity to the catalyst, these ILs are immobilized on suitable solid supports to embed the advantages of both ILs and solid support materials.[7] In this context, metal oxide nanoparticles (MONPs), serve as a suitable candidate because of their characteristic properties such as high surface areas, varying electronic structure, rich valence states, high surface area to volume ratio *etc.*[8] Because of these properties, MONPs found enormous applications in the field of nano-catalysis, electronics, optics and magnetic sensing, ceramic industry *etc.*[9] Transition MOs, especially rare earth MOs, such as Nd_2O_3 NPs have shown widespread applications in catalysis,[10] photonics,[11] advanced materials[12,13] and protective coatings.[14] Incorporation of ILs on the surface of MONPs introduce more desirable functionalities and stabilize the nano-catalytic systems with enhanced catalytic performance.[15] Moreover, IL functionalized nano-catalysts efficiently catalyze organic reactions such as epoxidation of alkenes,[16] aerobic oxidation of alcohols,[17] synthesis of cyclic carbonates from epoxides,[18] Heck reaction *etc.*[19]

Among the well known organic compounds, pyrrole and its derivatives are of great significance because of their widespread biological and commercial importance. These derivatives are widely used as intermediates in synthesis of dyes, photographic chemicals, pharmaceuticals, agrochemicals, perfumes *etc.*[20] Pyrrole possesses an imperative structural framework in wide range of biologically active organic scaffolds such as metal-cycloprodigiosin, spongiacidin B, longamide B *etc.*[20] (Fig. S1†). As they have great biological significance, therefore, need of the hour is to design some methodology for the synthesis of these

Department of Chemistry, Aligarh Muslim University, Aligarh 202002, Uttar Pradesh, India. E-mail: siddiqui_zeba@yahoo.co.in; zeba.ch@amu.ac.in

† Electronic supplementary information (ESI) available. See DOI: 10.1039/d0ra08812a

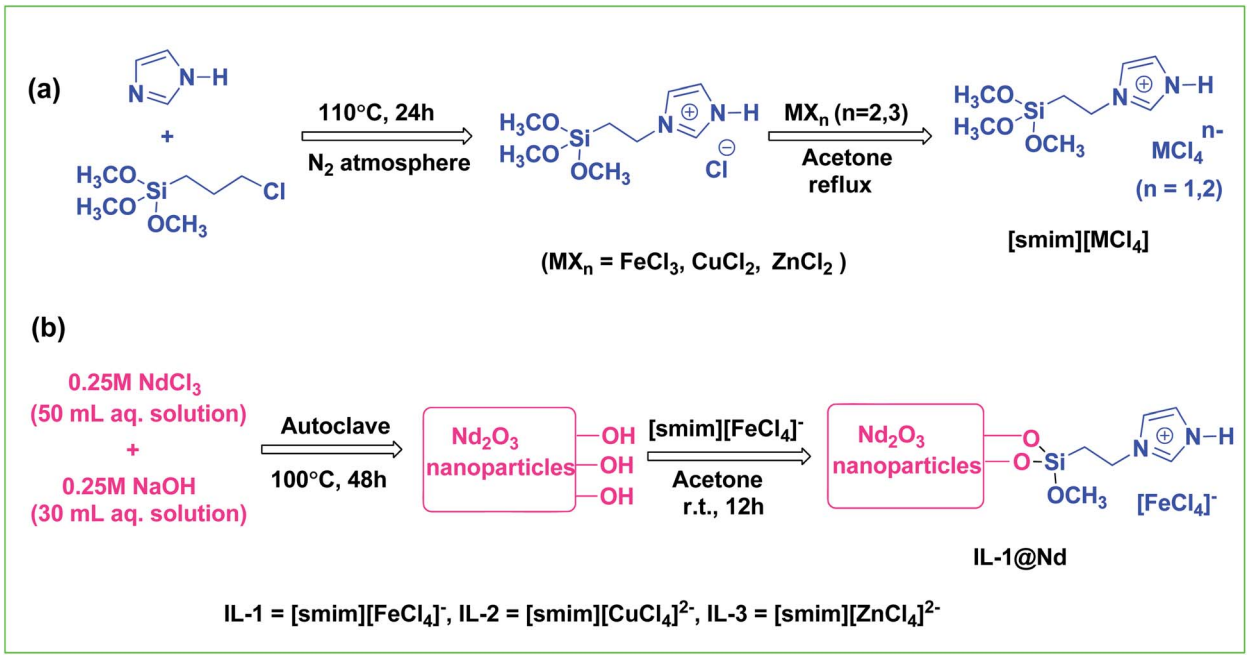

Scheme 1 (a) Schematic illustration of the general approach for the synthesis of [smim][MCl_4] (where M = Fe, Cu and Zn) (b) synthesis of IL-1@Nd.

compounds that is not only efficient but also better than earlier reported protocols from environmental and economical point of view.

As our ongoing research is focused on the synthesis of new heterogeneous catalytic systems,[21] in the present study, we have synthesized silica modified imidazolium based halometallic ILs; [smim][MCl_4] (M = Fe, Cu and Zn) and evaluated their acidic properties using potentiometric titration. A heterogeneous system, [smim][$FeCl_4$]$^-$@Nd_2O_3, has also been developed to catalyze the synthesis of a series of *N*-aryl indeno pyrrole derivatives. The present methodology includes detailed characterization of synthesized materials and evaluation of their acidic and catalytic properties. Sustainable pathways are used for the synthesis of organic scaffolds as confirmed from green metric evaluation.

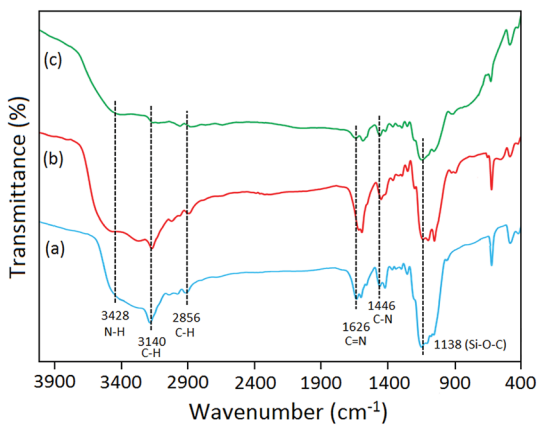

Fig. 1 FTIR spectrum of (a) IL-1 (b) IL-2 and (c) IL-3.

2. Results and discussion

2.1 Preparation and characterization of catalyst

The synthetic strategy for [smim][MCl_4] (where M = Fe, Cu and Zn) and [smim][$FeCl_4$]$^-$@Nd_2O_3 were represented in Scheme 1. Three ILs [smim][$FeCl_4$]$^-$, [smim][$CuCl_4$]$^{2-}$ and [smim][$ZnCl_4$]$^{2-}$ were abbreviated as IL-1, IL-2 and IL-3 respectively (Fig. S2†) whereas IL modified nano-catalyst, [smim][$FeCl_4$]$^-$@Nd_2O_3, was abbreviated as IL-1@Nd. The structure of IL-1@Nd was thoroughly characterized by various techniques such as Fourier transform infrared (FTIR) spectroscopy,

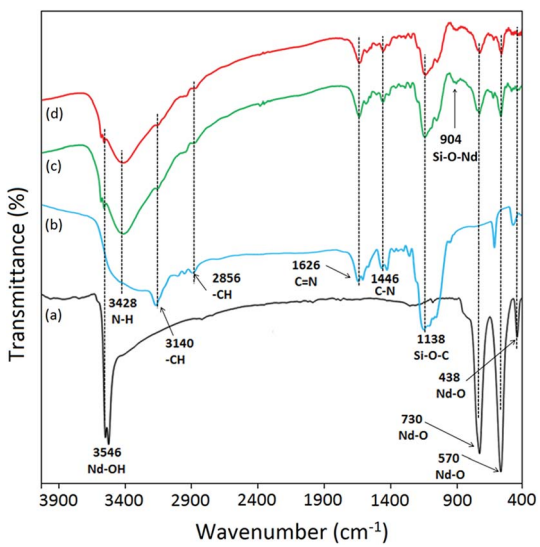

Fig. 2 FTIR spectrum of (a) Nd_2O_3 NPs (b) IL-1 (c) IL-1@Nd and (d) recycled catalyst.

ultraviolet-visible (UV-vis) DRS, Raman spectroscopy, Scanning Electron Microscope/Energy Dispersive X-ray (SEM/EDX), elemental mapping, Powder X-ray diffraction (XRD), Transmission Electron Microscope (TEM), Thermal Gravimetric (TG) and X-ray photoelectron spectroscopy (XPS) and electron paramagnetic resonance (EPR) analyses.

2.1.1 FTIR analysis. Imidazolium IL, (IL-1) (Fig. 1a), showed strong vibrational bands for N–H and C–H stretching modes of imidazole ring at 3428 cm^{-1} and 3140 cm^{-1} respectively.[22] The presence of alkyl chain was shown by the peak at 2856 cm^{-1} attributing to C–H stretching mode of vibration of CH_2 group.[23] The peaks arising at 1626 cm^{-1}, 1446 cm^{-1} and 1138 cm^{-1} were assigned to the vibrational modes of C=N, C–N, and Si–O–C respectively.[24] In, FTIR spectrum of IL-2 (Fig. 1b) and IL-3 (Fig. 1c) most of the vibrational bands were lying in the same region as observed in IL-1. It was due to the fact that halometallic anions (only difference in all ILs) were observed in either Far-IR or can be distinguished from Raman analysis.

The FTIR spectrum of Nd_2O_3 NPs displayed characteristic bands at 3546 cm^{-1}, 730 cm^{-1}, 570 cm^{-1}, and 438 cm^{-1} corresponding to stretching vibrational mode of –OH, and Nd–O bonds (Fig. 2a).[25] In the FTIR spectrum of IL-1, the characteristic bands for NH, CH (ring), CH (alkyl chain), C=N, C–N and Si–O–C were observed at 3428 cm^{-1}, 3140 cm^{-1}, 2856 cm^{-1}, 1626 cm^{-1}, 1446 cm^{-1}, 1138 cm^{-1} respectively (Fig. 2b). The FTIR spectrum of IL-1@Nd contained the vibrational bands of both IL and Nd_2O_3 NPs as shown in Fig. 2c. Only one new band was observed at 904 cm^{-1} due to the stretching vibration of Si–O–Nd bond.[26]

2.1.2 Raman analysis. The normalized Raman spectra of IL-1, IL-2, IL-3 and IL-1@Nd were obtained in the region of 100–600 cm^{-1} and depicted in Fig. 3. The strong band at 332 cm^{-1} originated from $[FeCl_4]^-$ of IL-1 due to symmetric stretching vibration of A1 mode in Fe–Cl bond (Fig. 3a).[27] Moreover, the absence of any other significant band eliminated the possibility of formation of $[Fe_2Cl_7]^-$ ion. The Raman spectrum of IL-2

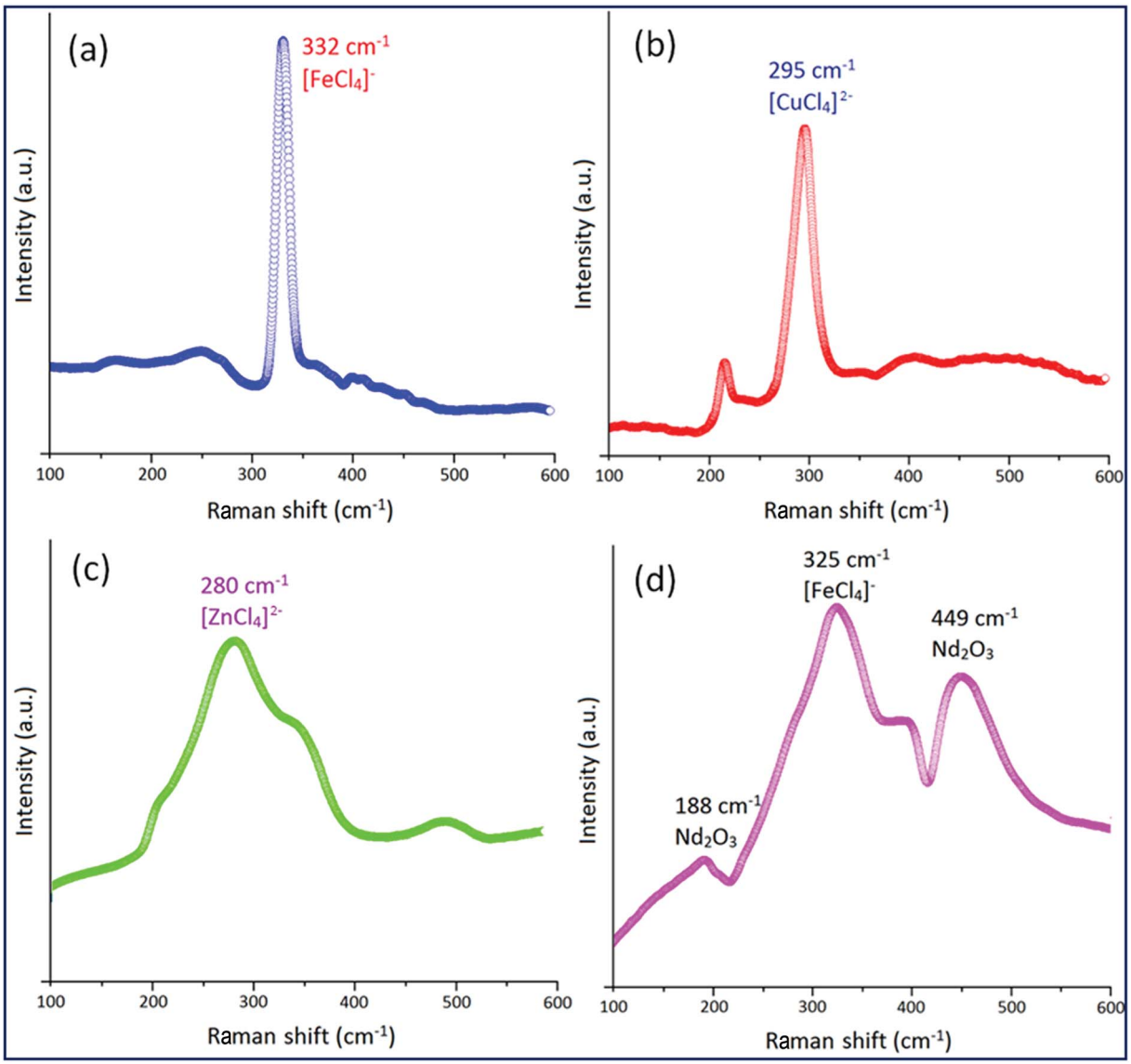

Fig. 3 Normalized Raman spectrum of (a) IL-1 (b) IL-2 (c) IL-3 and (d) IL-1@Nd.

showed sharp peak at 295 cm^{-1} corresponding to the symmetric stretching of Cu–Cl bond in $[CuCl_4]^{2-}$ ion (Fig. 3b).[28] The presence of $[ZnCl_4]^{2-}$ ion in IL-3 was confirmed from the band located at 280 cm^{-1} due to Zn–Cl stretching mode of vibration (Fig. 3c).[29] In the Raman spectrum of IL-1@Nd (Fig. 3d), characteristic bands of IL-1 and Nd_2O_3 NPs were observed. The peaks at188 cm^{-1} and 449 cm^{-1} were assigned to F_g mode and combination mode of A_g + E_g of Nd_2O_3 NPs whereas a sharp band at 325 cm^{-1} assured the presence of $[FeCl_4]^-$ of IL-1.[30]

2.1.3 DR-UV-vis analyses. DR-UV-vis spectrum of Nd_2O_3 NPs, IL-1, IL-2, IL-3 and IL-1@Nd were displayed in Fig. S3.† The DR-UV-vis spectrum of Nd_2O_3 NPs showed an absorption band at 529 nm which was in good agreement with earlier report (Fig. S3a†).[31] In all three ILs, absorption bands due to imidazole ring were observed in the range of 200–300 nm^1 (Fig. S3b–d†).[32] The DRS spectra of IL-1, IL-2 and IL-3 were distinguished by the bands due to $[MCl_4]$ ion (where M = Fe, Cu and Zn). The absorption peak for $[FeCl_4]^-$, $[CuCl_4]^{2-}$ in IL-1 and IL-2 and were observed at 340 nm and 530 nm respectively (Fig. S3b and c†).[33] However, no such absorption band was observed in the region of 200–600 nm in case of IL-3 (Fig. S3d†). In the DR-UV-vis spectrum of IL-1@Nd_2O_3, four absorption bands due to imidazolium cation, $[FeCl_4]$ and Nd_2O_3 NPs were observed at 222 nm and 294 nm, 346 nm and 521 nm respectively indicating the formation of desired catalytic system *i.e.* IL-1@Nd (Fig. S3e†).

2.1.4 SEM and TEM analysis. The morphological study of Nd_2O_3 and IL-1@Nd was performed using SEM and TEM analyses (Fig. 4). The morphology of Nd_2O_3 NPs showed spherical shaped particles (Fig. 4a). In the SEM image of IL-1@Nd (Fig. 4b), Nd_2O_3 NPs were decorated with IL-1 showing the successful incorporation of IL on the surface of Nd_2O_3 NPs. TEM image of Nd_2O_3 NPs showed the same morphology (spherical shape) with overlapping of few NPs (Fig. 4c). The image analysis was performed using ImageJ software and the average sizes of particles were found to be 34 ± 5 nm. The clear distribution of IL-1 on the surface of Nd_2O_3 NPs was further confirmed by TEM analysis (Fig. 4d).

2.1.5 EDX/mapping analysis. To investigate the presence of each element in IL-1@Nd, EDX analysis was performed and corresponding results were shown in Fig. S4.† The data revealed that all the constituent elements (C, O, Si, N, Nd, Cl, and Fe) were present as expected from the proposed catalytic system (Fig. S4a†). Further, the distribution of these elements throughout the catalyst was obtained from elemental mapping images of each element (Fig. S4b–h†). These images confirmed the uniform distribution of each individual element in the catalyst.

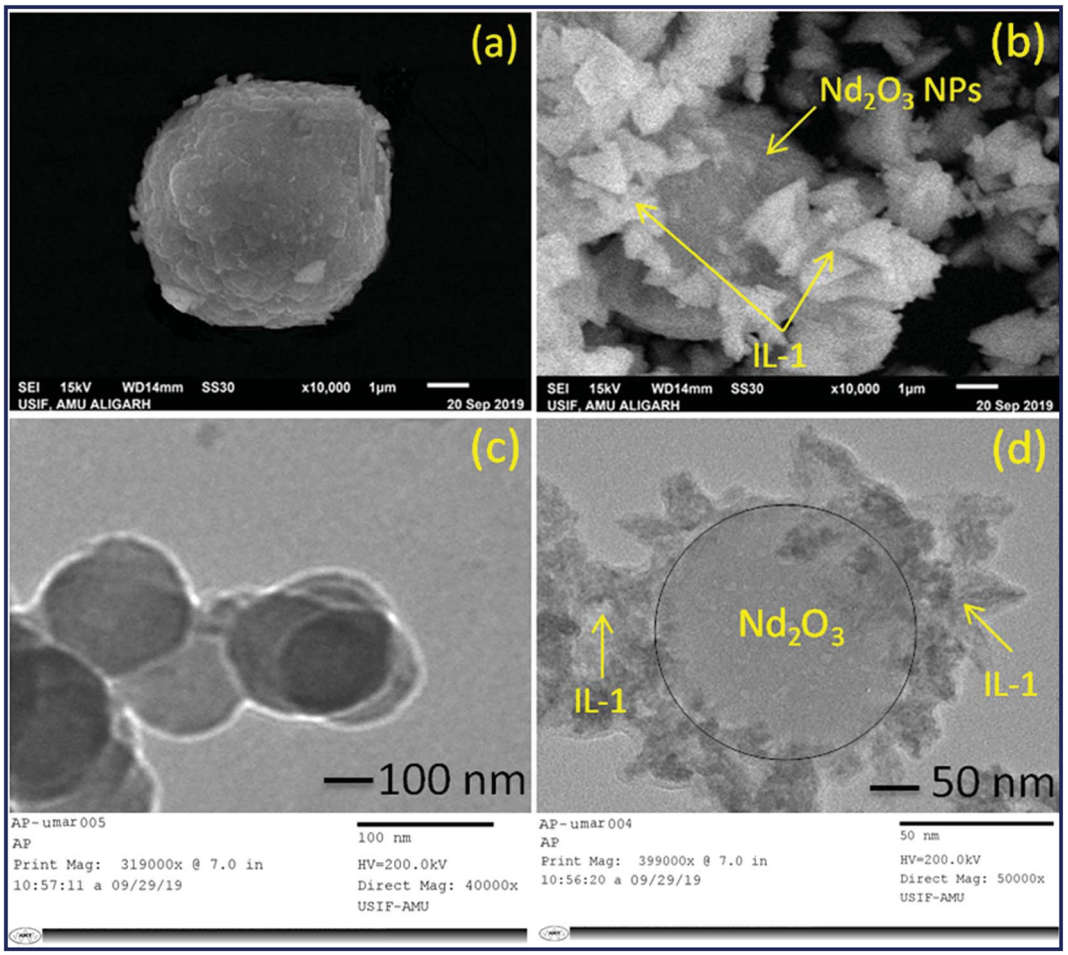

Fig. 4 SEM image of (a) Nd_2O_3 NPs and (b) IL-1@Nd; TEM image of (c) Nd_2O_3 and (d) IL-1@Nd.

2.1.6 XRD analysis. The XRD pattern of Nd_2O_3 NPs, IL-1@Nd and recycled catalyst were shown in Fig. 5. In the XRD spectrum of Nd_2O_3 NPs, sharp diffraction peaks at 13.98°, 16.4°, 20.76°, 24.82°, 26.5°, 27.2°, 28.18°, 31.24°, 34.20°, 36.78°, 39.42°, 40.43°, 46.5°, 50.10° were corresponding to (100), (011), (110), (101), (222), (002), (001), (411), (012), (431), (201), (160), (112) planes respectively (Fig. 5a).[34] These peaks confirmed the crystalline nature of synthesized Nd_2O_3 NPs. The XRD pattern of IL-1@Nd showed some additional peaks other than Nd_2O_3 NPs that may be due to the presence of IL-1 (Fig. 5b).

2.1.7 TG/DTG analysis. In order to study the thermal behavior of IL-1@Nd, TG-DTG analysis was performed (Fig. 6). The first weight loss of 7.43% at around 100 °C was attributed to the removal of physisorbed water molecules showing the hygroscopic nature of IL-1@Nd (Fig. 6). In the temperature range of 250–600 °C, a sequence of endothermic and exothermic effects with different weight losses were obtained in DTG and TG curves. The second weight loss (40.12%) between 406 °C to 453 °C was due to thermal degradation of IL from the surface of Nd_2O_3 NPs.[35] The third stage weight loss of 31.03% between 453 °C to 581 °C may be assigned to structural changes in Nd_2O_3. It clearly showed that IL-1@Nd was fairly stable up to 400 °C for catalytic activity. The DTG curve of IL-1@Nd showed a sharp exothermic peak at 455 °C and two shoulders at 250 °C and 836 °C which were assigned to oxidative decomposition of organic moieties present in the IL.[36]

2.1.8 Zeta potential analysis. The stability of nano-catalyst (IL-1@Nd) was investigated by zeta (ζ) potential analysis. As reported earlier, the minimum value of ζ potential for stability of nano-catalyst should be ±30 mV.[37] The halometallic IL functionalized catalyst (IL-1@Nd) showed ζ potential value of −40.32 mV. This confirmed that synthesized catalyst was fairly stable.

2.1.9 XPS analysis. XPS analysis was performed to elucidate the surface chemical compositions and chemical states of constituent elements in IL-1@Nd (Fig. 7). The photoelectron peaks for O 1s and N 1s were fitted by Gaussian function with

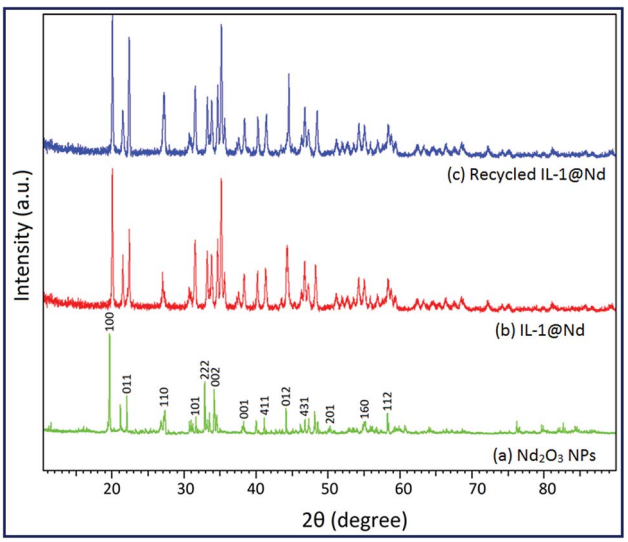

Fig. 5 XRD pattern of (a) Nd_2O_3 (b) IL-1@Nd (c) Recycled IL-1@Nd.

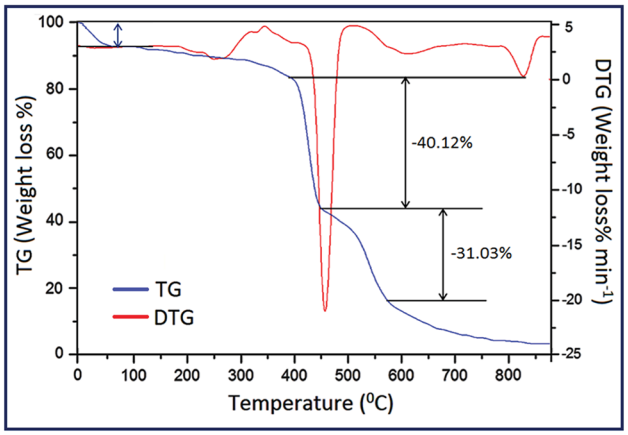

Fig. 6 TG-DTG curve of IL-1@Nd.

Shirely background subtraction in the present analysis. The XPS survey scan of IL-1@Nd clearly showed the predominant peaks for C, O, Si, Fe, Nd, N and Cl without other impurities (Fig. 7a). To extract further information, the narrow-scan XPS spectrum of C 1s (Fig. 7b), O 1s (Fig. 7c), Si 2p (Fig. 7d) and N 1s (Fig. 7e) level were recorded which consisted of broad peaks at binding energy (BE) values of 285.4 eV, 531.5 eV, 102.2 eV and 401.1 eV respectively.[21a] In (Fig. 7c), O 1s spectra indicated a relatively broad shape, which originates from the deconvolution of different contributions. Oxygen O 1s exhibited the one intense peak at binding energy (BE) of 531.5 eV due to the presence of O 1s core-level of O^{2-} state[38a] and also attributed to Si–O bonding.[38b] Another less intense peak at BE 529.7 eV was associated with Nd–O bonding in the sample matrix.[39] The deconvolution of N 1s spectra, exhibited three peaks at BE 401.1 eV, 399.5 eV and 398.3 eV which were attributed to N=C, N–C and N–H respectively.[40] The Fe $2p^3$, Nd $3d^5$ and Cl 2p level XPS spectrum were comprised of two characteristic peaks. In case of Fe $2p^3$ level, the peaks located at 712.4 eV and 725.1 eV were corresponding to the BE of Fe $2p_{3/2}$ (Fe^{3+}) and Fe $2p_{1/2}$ respectively (Fig. 7f).[41] Two peaks with BE of 983.2 eV and 1006.3 eV were attributed to the BE of $Nd_{5/2}$ and $Nd_{3/2}$ respectively (Fig. 7g).[42] In the narrow-scan XPS spectrum of Cl 2p level, a prominent peak at 199.6 eV and a shoulder at 197.5 eV were corresponding to the BE of Cl $2p_{1/2}$ and Cl $2p_{3/2}$ respectively (Fig. 7h).[25b] The analysis showed the weight% of Fe to be 4.23% in IL-1@Nd which corresponded to the loading amount of 0.79 mmol g^{-1} of catalyst.

2.1.10 EPR analysis. In order to confirm the oxidation state of Fe in $[FeCl_4]$ ion present in IL-1@Nd, X-band EPR analysis was performed. A sharp singlet at $g = 2.0412$ obtained in the EPR spectrum of IL-1@Nd assured the presence of Fe^{3+} (oxidation state of Fe = +3).[21a]

2.2 Measurement of acidity of synthesized materials by potentiometric titration

Acidity of solid acid catalysts can also be measured by potentiometric titration with an organic base. The acidic environment around the electrode membrane was examined and corresponding potential difference was measured. The electrode potential was used for the determination of acidic nature of

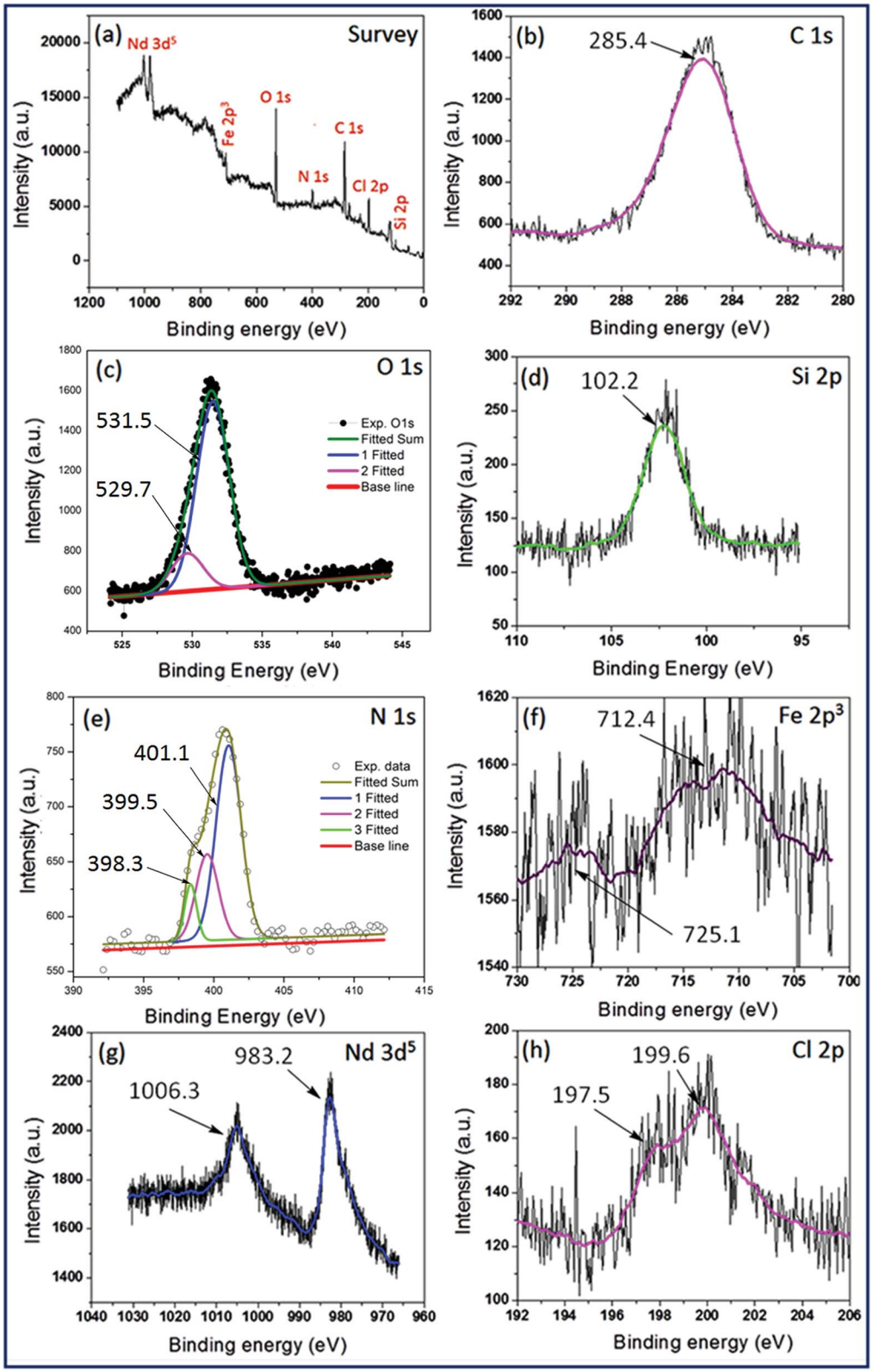

Fig. 7 (a) XPS survey spectrum of IL-1@Nd, high resolution XPS spectrum of (b) C 1s (c) O 1 s (d) Si 2p (e) Fe $2p^3$ (f) Nd $3d^5$ (g) N 1s and (h) Cl 2p.

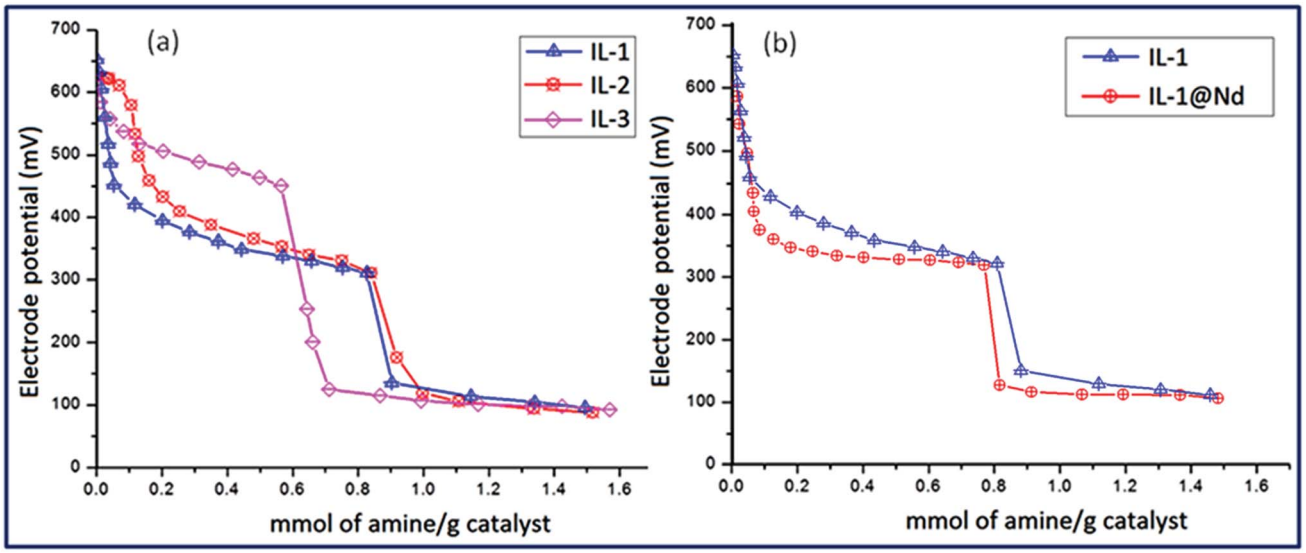

Fig. 8 Potentimetric titration curve of (a) IL-1, IL-2 and IL-3; (b) IL-1 and IL-1@Nd.

dispersed solid particles. The potentiometric titration curves were obtained for IL-1, IL-2 and IL-3 against *n*-butylamine to investigate the total number of acidic sites of titrated materials (Fig. 8). The acidic sites of materials were calculated by the peak heights of titration curve considering that the initial electrode potential (E_i) indicated the maximum strength of the acid sites. The electrode potential lying in the range of >100 mV corresponded to the material with very strong acidic sites, value of E in between $0 < E_i < 100$ mV were belonged to the material of significantly strong acidity and in the range of $-100 < E_i < 0$ mV were attributed to the materials having weak acid sites.[43] The results of titrated materials from Fig. 8a revealed that IL-1, IL-2 and IL-3 contained very strong acidic sites (>100 mV). The E_i values of IL-1 (654 mV), IL-2 (635 mV) and IL-3 (610 mV) showed that IL-1 had stronger acidic sites among the three which might be due to the availability of Fe^{3+} ion as confirmed by EPR and XPS analyses. When ILs were incorporated on the surface of Nd_2O_3 NPs, new species in the form of Si–O–Nd were generated as confirmed by FTIR spectroscopy and this might be the cause of decrement in acidity of IL functionalized materials.[44] As shown in Fig. 8b, acidity of IL-1@Nd (602 mV) was decreased in comparison to pure IL-1 (654 mV). It can also be due to the slight basic nature of Nd_2O_3 NPs as reported earlier.[45]

2.3 Evaluation of optimized reaction conditions for the synthesis of dihydroxyoxoindeno[1,2-*b*]pyrrole derivatives

In order to obtain the optimum reaction conditions for the synthesis of *N*-aryl indeno pyrrole derivatives, a set of experiments were carried out using a model reaction of dimedone **1a** (2 mmol), 4-chloroaniline **2a** (2 mmol) and ninhydrin **3** (2 mmol) to afford **4a** (Scheme 2). The main goal of these experiments was to maximize the product yield in shorter reaction time by adopting a sustainable synthetic route. The different parameters (role of catalyst and solvents, impact of temperature, effect of catalyst loading and support) were investigated thoroughly and the corresponding results were discussed below.

The very first task was to choose a suitable catalyst for the model reaction affording best results in terms of product yield and time. The model reaction was first tried in the absence of catalyst and did not proceed well after prolonged heating (Table

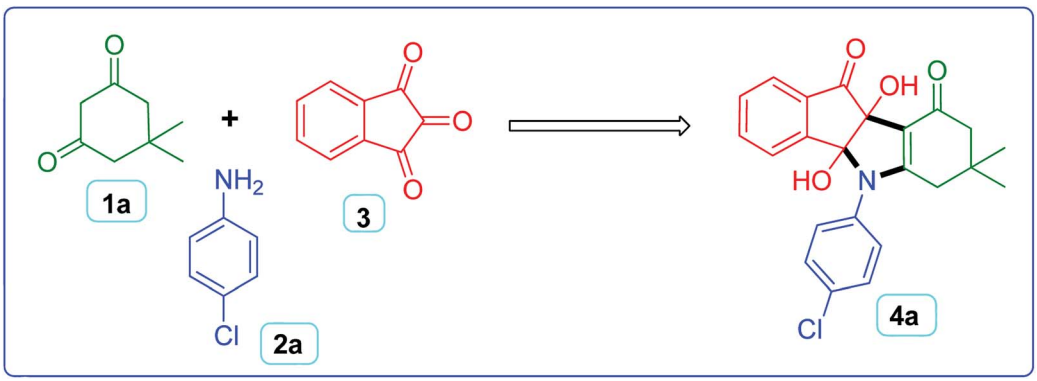

Scheme 2 Model reaction for the synthesis of **4a**.

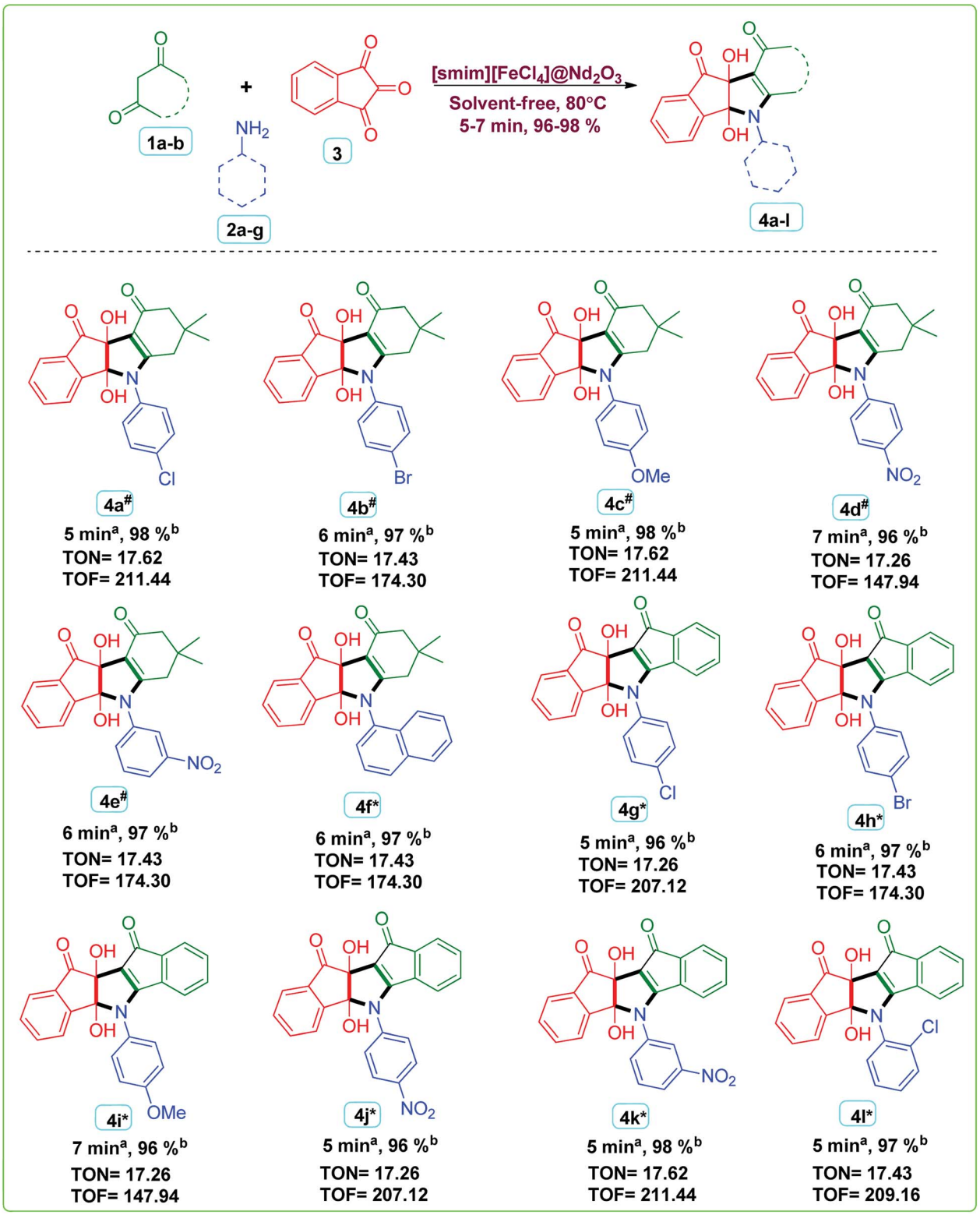

Scheme 3 IL-1@Nd catalyzed synthesis of indeno pyrrole derivatives. #Reported compounds.[46] *This work. [a]Reaction progress monitored by TLC. [b]Isolated yield.

1, entry 1). Then, reaction was carried out in the presence of silica-based imidazolium ILs and product was obtained in good to moderate yield (Table 1, entry 2–5). Using halometallic ILs as catalysts, yield of the product further enhanced (Table 1, entry 6–8). Out of three halometallic ILs used, IL-1 showed better activity producing 75% of the product (Table 1, entry 6). As an effort to introduce heterogeneity in the catalyst and taking into account the high surface area of the support materials, different

nano-materials were examined as catalyst support such as ZrO_2, SiO_2, Al_2O_3, La_2O_3, CeO_2 and Nd_2O_3 (Table 1, entry 9–14). It was observed that IL-1 immobilized Nd_2O_3 (IL-1@ Nd_2O_3) showed best result among all supports materials used for the analysis (Table 1, entry 14).

In order to choose the best solvent for model reaction, different protic and aprotic solvents (hexane, acetonitrile, tetrahydrofuran, dimethylsulfoxide, methanol and ethanol) were examined using model reaction (Table 1S,† entries 1–6). When reaction was carried out under solvent-free conditions, excellent yield of the product (98%) was obtained in very short reaction time (5 min) (Table 1S,† entries 7). The model reaction was also tested under different heating conditions to check the effect of temperature on reaction rate (Table 2S†). On increasing the temperature from 25 °C to 80 °C, rate of reaction also increased (Table 2S,† entries 1–4). It was observed from the results that 80 °C was sufficient to achieve best results because further increase in temperature did not affect the reaction rate. It was obvious to see to how much IL should be loaded on the surface of Nd_2O_3 NPs to achieve best catalytic performance. For that, different loading amount of IL-1 (v/w) was used and efficiency of catalysts was investigated (Table 3S†). The results revealed that 20% (v/w) loading amount was sufficient enough to catalyze the model reaction producing best result (Table 3S,† Entry 4). In order to check the effect of catalyst concentration on model reaction, different amounts of IL-1@Nd were employed and found that 50 mg of IL-1@Nd was enough to catalyze the reaction (Table 4S,† entry 5).

2.4 Catalytic reaction

A multicomponent reaction of dimedone/indanedione **1a-b** (2 mmol), aromatic amines **2a–g** (2 mmol) and ninhydrin **3** (2 mmol) were performed under solvent free reaction conditions using IL-1@Nd as a green heterogeneous catalyst to synthesize indeno pyrrole derivatives **4a–l** (Scheme 3). Turnover number (TON) and turnover frequency (TOF) were calculated to analyze the efficiency of the catalyst. The high TOF value showed that the IL-1@Nd was highly efficient to catalyze the multicomponent reaction. The TON values were found in the range of 17 whereas TOF values ranged from 147 h^{-1} to 211 h^{-1}. The high TOF values showed that IL-1@Nd was efficient for the synthesis of indeno pyrroles.

2.5 Green matrix for synthesized compounds (4a–l)

The sustainability of the reaction was assessed by green matrix analysis. The parameters of green matrix were atom economy (AE), carbon efficiency (CE), reaction mass intensity (RME), process mass intensity (PMI), overall efficiency (OE), solvent intensity (SI) and E-factor. The calculated parameters showed that the synthesized compounds were acceptable from green perspective showing %AE, %CE, %RME and %OE values closed to 100%. The results (Table S5†)[48] produced high AE (84.21–86.69%), high OE (87.24–94.28%) and low E-factor (3.61–4.69) which was a clear indication of energy sustainable synthetic methodology[47] used in present study.

Table 1 Optimization of reaction conditions for model reaction[a]

Entry	Catalyst	Time[b]	Yield[c] (%)
1	No catalyst	24 h	26
2	[smim]Cl^- (10 mol%)	4.5 h	54
3	[smim]CH_3COO^- (10 mol%)	5 h	43
4	[smim]$H_2PO_4^-$ (10 mol%)	4.5 h	48
5	[smim]ClO_4^- (10 mol%)	4 h	50
6	**IL-1** (10 mol%)	**1.5 h**	**75**
7	IL-2 (10 mol%)	3 h	62
8	IL-3 (10 mol%)	3.5 h	60
9	IL-1@ZrO_2 (50 mg)	48 min	80
10	IL-1@SiO_2 (50 mg)	40 min	84
11	IL-1@Al_2O_3 (50 mg)	45 min	82
12	IL-1@La_2O_3 (50 mg)	35 min	80
13	IL-1@CeO_2 (50 mg)	30 min	82
14	**IL-1@ Nd_2O_3** (50 mg)	**5 min**	**98**

[a] Reaction conditions: dimedone **1a** (2 mmol), 4-chloroaniline **2a** (2 mmol), ninhydrin **3** (2 mmol), catalysts, solvent-free, T = 80 °C. [b] Reaction progress monitored by TLC. [c] Isolated yield.

2.6 Recycling study of IL-1@Nd for the synthesis of 4a

In order to check the reusability of the catalyst, a representative reaction of dimedone **1a**, aniline **2a** and 1,3-indanedione **3** in the presence of 50 mg of IL-1@Nd under solvent free conditions at 80 °C was employed. When reaction reached completion (as monitored by TLC), ethyl acetate was added to the reaction mixture to separate the organic compound **4a**. The catalyst was filtered, washed with ethanol, dried in oven at 60 °C for 1 h and reused. The same experiment was repeated for five successive runs and recycling data were recorded. The investigation of catalyst structure after five runs was done using several techniques such as FTIR, SEM, XRD and acidic sites were measured by potentiometric titration. In the FTIR spectrum of recycled IL-1@Nd, all characteristic bands such as 3548 cm^{-1} (Nd–OH), 3426 cm^{-1} (–NH), 3143 cm^{-1} (–CH), 2852 cm^{-1} (–CH), 1628 cm^{-1} (C=N), 1440 cm^{-1} (C–N), 1132 cm^{-1} (Si–O–C), 900 cm^{-1} (Si–O–Nd), 732 cm^{-1} (Nd–O), 574 cm^{-1} (Nd–O) and 430 cm^{-1} (Nd–O) were present (Fig. 1d). XRD spectrum showed same diffraction pattern as that of fresh catalyst (Fig. 5c). SEM (Fig. S5a†) analysis displayed no morphological change after catalytic use. The potentiometric titration of recycled IL-1@Nd was compared with fresh IL-1@Nd (Fig. S5b†) and found that all active acidic sites were present in the catalyst during the course of reaction. The results of these techniques showed that no significant changes occurred in the structure of catalyst after five successive catalytic runs (Fig. S6†).

3. Experimental

3.1 Synthesis of [smim][MCl_4] and IL-1@Nd

The catalyst was synthesized in two steps as shown in Scheme 1. First, IL [smim][MCl_4] (M = Fe, Cu and Zn) was synthesized by using our previous procedure.[21a] In the second step, Nd_2O_3 NPs were synthesized by hydrothermal process. In a typical run, 50 mL aqueous solution of 0.25 M $NdCl_3$ was mixed with 30 mL aqueous solution of 0.25 M NaOH and kept in autoclave for 48 h at 100 °C. The bluish white colored aqueous suspension was

formed which was filtered and washed thrice with double distilled water and acetone and dried in oven at 60 °C for 24 h to get bluish white colored powder of Nd_2O_3 NPs. The as synthesized Nd_2O_3 NPs was calcined at 400 °C for 3 h. 500 mg of Nd_2O_3 NPs were mixed with equal amount of IL-1 in acetone and stirred for 12 h at room temperature to obtain final catalyst IL-1@Nd.

3.2 General procedure for the synthesis of dihydroxyoxoindeno[1,2-*b*]pyrrole derivatives

Dimedone/indanedione **1a-b** (2 mmol), aromatic amines **2a–g** (2 mmol) ninhydrin **3** (2 mmol), and were taken in 50 ml round bottom flask containing 10 mL ethanol and stirred at 80 °C for specified time period. In most of the reaction, white color solid was settled at the bottom. The reaction mixture along with solid acid catalyst was dissolved in ethyl acetate to separate the organic compounds and catalyst. The catalyst remained insoluble in ethyl acetate and separated by simple filtration, dried in oven for 4 h at 60 °C and reused. The organic compounds (**4a–l**) were obtained by evaporation of ethyl acetate under reduced atmosphere, dried and recrystallized from ethanol : ethyl acetate (1 : 5) mixture.

4. Conclusion

A series of three ILs (IL-1, IL-2 and IL-3) having different metal ions (Fe, Cu and Zn respectively) was synthesized and evaluated for acidic properties by acid–base potentiometric titration using *n*-butyl amine as an organic base. A heterogeneous catalyst (IL-1@Nd) was designed for catalytic potential towards synthesis of indeno pyrrole derivatives showing better performance in terms of product yield (96–98%) and reaction time (5–7 min). The results of green metric analysis confirmed the greenness of present synthetic methodology producing high AE (84.21–86.69%) with low E-factor (3.61–4.69). The notable features of present study were sustainable synthetic process, high product yield, short reaction time and good recyclability of catalyst.

Conflicts of interest

There are no conflicts of interest to declare.

Acknowledgements

The author (Mohd Umar Khan) gratefully acknowledge the financial assistance in the form of Maulana Azad National Fellowship (MANF), Ministry of Minority Affairs, U.G.C. The authors would also like to thank DRS II (New Delhi), USIF, A.M.U. for SEM/EDX and TEM analyses, Department of Physics (A.M.U. Aligarh) for XRD analysis, and IIT Roorkee for XPS analysis.

References

1 D. Zheng, T. Wang, X. Zhu, C. Chen, T. Ren, L. Wang and J. Zhang, *Mol. Syst. Des. Eng.*, 2018, **3**, 348–356.
2 M. Rahman, *Recent Advances in Ionic Liquids*, BoD–Books on Demand, 2018.
3 J. Estager, J. D. Holbrey and M. Swadźba-Kwaśny, *Chem. Soc. Rev.*, 2014, **43**, 847–886.
4 N. Sahiner, T. Turhan and L. A. Lyon, *Energy*, 2014, **66**, 256–263.
5 (*a*) M. P. Singh, R. K. Singh and S. Chandra, *J. Phys. Chem. B*, 2011, **115**, 7505–7514; (*b*) T. Sasaki, M. Tada, C. Zhong, T. Kume and Y. Iwasawa, *J. Mol. Catal. A: Chem.*, 2008, **279**, 200–209.
6 N. Sahiner, S. Demir and S. Yildiz, *Colloids Surf., A*, 2014, **449**, 87–95.
7 M. H. Valkenberg and W. F. Hölderich, *Green Chem.*, 2002, **4**, 88–93.
8 M. T. Reetz and M. Maase, *Adv. Mater.*, 1999, **11**, 773–777.
9 G. Oskam, *J. Sol-Gel Sci. Technol.*, 2006, **37**, 161–164.
10 G. Tosun and H. F. Rase, *Ind. Eng. Chem. Prod. Res. Dev.*, 1972, **11**, 249–260.
11 W. Que, C. H. Kam, Y. Zhou, Y. L. Lam and Y. C. Chan, *J. Appl. Phys.*, 2001, **90**, 4865–4867.
12 J. Singh, N. C. Soni and S. L. Srivastava, *Bull. Mater. Sci.*, 2003, **26**, 397–399.
13 F. Delorme, C. Harnois, I. Monot-Laffez and G. Desgardin, *Phys. C*, 2002, **372**, 1127–1130.
14 S. Chevalier, G. Bonnet and J. P. Larpin, *Appl. Surf. Sci.*, 2000, **167**, 125–133.
15 (*a*) H. Li and Y. Bian, *Nanotechnology*, 2009, **20**, 145502; (*b*) J. Ling, Y. Sang and C. Z. Huang, *J. Pharm. Biomed. Anal.*, 2008, **47**, 860–864; (*c*) H. Li, Y. Yao, C. Han and J. Zhan, *Chem. Commun.*, 2009, 4812–4814.
16 K. Yamaguchi, C. Yoshida, S. Uchida and N. Mizuno, *J. Am. Chem. Soc.*, 2005, **127**, 530–531.
17 R. Ciriminna, P. Hesemann, J. J. E. Moreau, M. Carraro, S. Campestrini and M. Pagliaro, *Chem. - Eur. J.*, 2006, **12**, 5220–5224.
18 S. M. Sadeghzadeh, *Green Chem.*, 2015, **17**, 3059–3066.
19 B. Karimi and D. Enders, *Org. Lett.*, 2006, **8**, 1237–1240.
20 R. Kaur, V. Rani and V. Abbot, *J. Pharm. Chem. Chem. Sci.*, 2017, **1**(1), 17–32.
21 (*a*) M. U. Khan, S. Siddiqui, W. A. Khan and Z. N. Siddiqui, *New J. Chem.*, 2020, **44**, 4822–4833; (*b*) M. U. Khan and Z. N. Siddiqui, *ACS Omega*, 2018, **3**, 10357–10364; (*c*) S. Siddiqui and Z. N. Siddiqui, *Appl. Organomet. Chem.*, 2019, e5161; (*d*) S. Siddiqui, M. U. Khan and Z. N. Siddiqui, *ACS Sustainable Chem. Eng.*, 2017, **5**, 7932–7941; (*e*) S. Siddiqui and Z. N. Siddiqui, *Catal. Lett.*, 2018, **0**, 0; (*f*) R. A. Rather, M. U. Khan and Z. N. Siddiqui, *RSC Adv.*, 2020, **10**, 818–827; (*g*) M. U. Khan, S. Siddiqui and Z. N. Siddiqui, *ACS Omega*, 2019, **4**, 7586–7595.
22 (*a*) Z. S. Qureshi, K. M. Deshmukh, M. D. Bhor and B. M. Bhanage, *Catal. Commun.*, 2009, **10**, 833–837; (*b*) S. Udayakumar, M.-K. Lee, H.-L. Shim, S.-W. Park and D.-W. Park, *Catal. Commun.*, 2009, **10**, 659–664.
23 M. Ghorbani, S. Noura, M. Oftadeh and M. A. Zolfigol, *RSC Adv.*, 2015, **5**, 55303–55312.
24 (*a*) P. Aghamkar, S. Duhan, M. Singh, N. Kishore and P. K. Sen, *J. Sol-Gel Sci. Technol.*, 2008, **46**, 17–22; (*b*)

Q. Lyu, H. Yan, L. Li, Z. Chen, H. Yao and Y. Nie, *Polymers*, 2017, **9**, 447.

25 (*a*) S. Zinatloo-Ajabshir, S. Mortazavi-Derazkola and M. Salavati-Niasari, *J. Mol. Liq.*, 2017, **234**, 430–436; (*b*) M. S. Lembang, Y. Yulizar, S. Sudirman and D. O. B. Apriandanu, in *AIP Conference Proceedings*, AIP Publishing LLC, 2018, vol. 2023, p. 20093.

26 M. C. Smith, Y. Xiao, H. Wang, S. J. George, D. Coucouvanis, M. Koutmos, W. Sturhahn, E. E. Alp, J. Zhao and S. P. Cramer, *Inorg. Chem.*, 2005, **44**, 5562–5570.

27 M. S. Sitze, E. R. Schreiter, E. V Patterson and R. G. Freeman, *Inorg. Chem.*, 2001, **40**, 2298–2304.

28 R. E. Del Sesto, T. M. McCleskey, A. K. Burrell, G. A. Baker, J. D. Thompson, B. L. Scott, J. S. Wilkes and P. Williams, *Chem. Commun.*, 2008, 447–449.

29 N. Trendafilova, G. S. Nikolov, R. Kellner and G. Bauer, *Vib. Spectrosc.*, 1994, **6**, 351–362.

30 (*a*) B. Umesh, B. Eraiah, H. Nagabhushana, B. M. Nagabhushana, G. Nagaraja, C. Shivakumara and R. P. S. Chakradhar, *J. Alloys Compd.*, 2011, **509**, 1146–1151; (*b*) B. Umesh, B. Eraiah, H. Nagabhushana, S. C. Sharma, D. V Sunitha, B. M. Nagabhushana, C. Shivakumara, J. L. Rao and R. P. S. Chakradhar, *Spectrochim. Acta, Part A*, 2012, **93**, 228–234.

31 S. Mortazavi-Derazkola, S. Zinatloo-Ajabshir and M. Salavati-Niasari, *J. Mater. Sci.: Mater. Electron.*, 2015, **26**, 5658–5667.

32 F. Peral and E. Gallego, *J. Mol. Struct.*, 1997, **415**, 187–196.

33 F. A. Yassin, F. Y. El Kady, H. S. Ahmed, L. K. Mohamed, S. A. Shaban and A. K. Elfadaly, *Egypt. J. Pet.*, 2015, **24**, 103–111.

34 R. B. Yu, K. H. Yu, W. Wei, X. X. Xu, X. M. Qiu, S. Liu, W. Huang, G. Tang, H. Ford and B. Peng, *J. Adv. Mater.*, 2007, **19**, 838–842.

35 Y. Yoshida and G. Saito, *J. Mater. Chem.*, 2006, **16**, 1254–1262.

36 B. Huang, C. Huang, J. Chen and X. Sun, *J. Alloys Compd.*, 2017, **712**, 164–171.

37 A. Komalam, L. G. Muraleegharan, S. Subburaj, S. Suseela, A. Babu and S. George, *Int. Nano Lett.*, 2012, **2**, 26.

38 (*a*) D. Xu, D. Fan and W. Shen, *Nanoscale Res. Lett.*, 2013, **8**, 46; (*b*) Y. Zhang, L. Zhu, L. Chen, L. Liu and G. Ye, *Rev. Adv. Mater. Sci.*, 2019, **58**, 32–37.

39 A. Wahid, A. M. Asiri and M. M. Rahman, *Appl. Surf. Sci.*, 2019, **487**, 1253–1261.

40 Y. Ye, D. Zhang, T. Liu, Z. Liu, J. Pu, W. Liu, H. Zhao, X. Li and L. Wang, *Carbon*, 2019, **142**, 164–176.

41 J. C. Yoon, J.-S. Lee, S.-I. Kim, K.-H. Kim and J.-H. Jang, *Sci. Rep.*, 2013, **3**, 1788.

42 M. M. Rahman, A. Wahid, M. M. Alam and A. M. Asiri, *Mater. Today Commun.*, 2018, **16**, 307–313.

43 E. Rafiee, M. Joshaghani, S. Eavani and S. Rashidzadeh, *Green Chem.*, 2008, **10**, 982–989.

44 E. Rafiee and S. Eavani, *Green Chem.*, 2011, **13**, 2116–2122.

45 S. Sato, R. Takahashi, M. Kobune, H. Inoue, Y. Izawa, H. Ohno and K. Takahashi, *Appl. Catal., A*, 2009, **356**, 64–71.

46 (*a*) M. Kour, M. Bhardwaj, H. Sharma, S. Paul and J. H. Clark, *New J. Chem.*, 2017, **41**, 5521–5532; (*b*) K. Pradhan, S. Paul and A. R. Das, *RSC Adv.*, 2015, **5**, 12062–12070.

47 R. A. Sheldon, *ACS Sustainable Chem. Eng.*, 2018, **6**, 32–48.

48 J. Safari, S. H. Banitaba and S. D. Khalili, *J. Mol. Catal. A: Chem.*, 2011, **335**, 46–50.